MODEL CAVITY STUDIES FOR TANK DESIGN AND ON TANK FABRICATION

H. Baba*, H. Hirakawa**, T. Nishikawa**,
S. Okumura*, J. Tanaka* and Y. Tao**

* Institute for Nuclear Study, University of Tokyo,
Tanashi, Tokyo, Japan

** Department of Physics, University of Tokyo,
Bunkyo, Tokyo, Japan

1. Model Cavities for the Design of the First Tank

The initial evaluation of cavity dimensions of the injector linac for the Proton Synchrotron Project in Japan was made by using the data of MURA Linac Cavity Calculation[1]. The reasons for using these data were that they were summarized conveniently for calculating the linac dimensions and that their reliability was already confirmed by experiments[2].

As the beam quality at the low energy part of the proton linac is most determinative to the overall linac performance, we have concentrated our design study on the first tank in which protons will be accelerated from 0.75 MeV to 10 MeV.

The geometric dimensions of the MURA data which we have used for the first tank are listed in Table I. To obtain the final design values, we constructed two model cavities for the first tank. The first type is the nearly full-size model consisting of several uniform cells, and the second is a half-size model of the whole tank.

For these model cavities, we measured the field distributions and the resonant frequencies. Since the model cavities were not evacuated, the measured resonant frequencies were corrected for the dielectric constant of air. We also made the correction of scaling factor to obtain the values for original dimensions. In this paper, we present the measured values with these corrections. The resonant frequency means that of TM_{010} mode, if not specified.

1 - 1 Model Cavity of Type I

To determine the dimension of each cell which resonate at the design frequency (201.25 MHz), we made the Type I model cavity. The outer cylinder of this cavity has a inner diameter of 88 cm and a length of 26 cm. Both the outer cylinder and the stems are made of brass and the drift-tubes are made of aluminium within the accuracy of 0.01 mm. A number of uniform drift-tubes are inserted into the cavity; the number can be chosen as an integer or a half integer between 4.5 and 1.5. In case the cavity has a half-cell, a half-drift-tube and two half-stems are attached to one end plate. Each drift tube is supported by two stems vertically from the top of the cavity and horizontally from the left or right side alternately.

As the horizontal stems can be easily taken off without giving disturbance to the alignment of the drift-tubes, we can measure the shifts of resonant frequency due to stems. To obtain the effect of small changes in the drift-tube diameter, a set of drift-tubes of slightly different diameters are also prepared.

The dimensions of model cavity are tabulated in Table II. Corresponding to the ratio of the inner diameter of the model cavity to that in Table I, all dimensional parameters are given by multiplying those obtained from the interpolations of the MURA data by a factor of 88/94.

1 - 2 Frequency Measurements for the Type I Model Cavity

The measured resonant frequencies of the Type I model cavity are shown in Fig. 1. The bars in Fig. 1 give the errors estimated from the mechanical accuracies.

The shifts of the resonant frequency due to stems are plotted in Fig. 2 together with the values calculated by Parzen[3]. The agreements between the experimental values and calculated ones are good for larger cell-length, but for shorter cell-length the experiments give smaller values than the calculations. Although the measurement is impossible with no stems, the unperturbed resonant frequency can be estimated by assuming that the shift is proportional to the cross section of the stems. These unperturbed frequencies can be compared with the design frequency of 201.25 MHz for which the dimensions was determined by using MURA data. The experimental frequencies deviate systematically from the design frequency in a manner similar to those obtained by Young[2]. The derivatives of the resonant frequency with respect to drift-tube diameter were also measured and plotted in Fig.3. The changes of drift-tube diameter for this measurement were from 0.5 cm to 0.2 cm according to the increase of cell length. This did not cause any appreciable changes in transit-time-factors.

1 - 3 Model Cavity of Type II

In order to study the field excitations and the distributions, we constructed the Type II model

cavity, which has the half-size dimensions of the design values of the first tank.

A picture of the Type II model cavity is shown in Fig. 4. The materials of this cavity are the same as those of Type I. The cavity consists of 56 unit cell elements, each unit having one drift-tube. Putting the end plate at any gap center between two drift-tubes, we can investigate RF properties for the cell assembly of arbitrary number and any portion of the tank. RF power can be fed not only from the end plate as in the case of the Type I, but also from various positions by using the feed and pick-up holes on each cell cylinder.

As in the AGS Converstion Linac of Brookhaven, the axial average field was taken as

$$E = (1.5 + 0.09\ z(m))\ \ MV/m \qquad (1)$$

in the design stage. The cell dimensions were determined by making corrections to the MURA data, based on the frequency measurements for the Type I cavity, so that each cell resonates at the design frequency (201.25 ± 0.1) × 2 MHz. As a result, the drift-tubes were divided into five groups stepped within the difference of 0.1 cm in diameter. The transit-time-factors do not change by such a dimensional change, so that the effects on the beam dynamics need not to be taken into account.

1 - 4 Frequency Measurements for the Type II Model Cavity

The resonant frequency of the whole cavity was 201.12 MHz. The reason of the deviation from the design value (201.25 MHz) has not been clear, but it is supposed to be caused by the machining errors or more essentially by the effect of coupling the cell units slightly differing in shape. The resonant frequencies of several higher-modes were also measured. The results were as follows:

TM_{011} mode 202.17 MHz
TM_{012} mode 205.27 MHz
TM_{013} mode 210.29 MHz .

The dispersion curve is given in Fig. 5. Frequencies of the modes associated with the stem resonance[4] were also measured. They are shown in Fig. 6.

1 - 5 Measurements of Cavity Field

The measurements of axial electric field along the model cavities have been made by the frequency perturbation method. We used alminium balls of 8 mm in diameter for the Type I cavity and 4 mm for the Type II cavity.

The ball was fastened onto a thin nylon thread, which was tightly stretched with a uniform tension and slided along the axis of the cavity by a synchronous motor. The block diagram of the measuring system is shown in Fig. 7. The driving speed of the ball was 2 mm/sec and the frequency was measured three times in every one second.

An example of the plots of measured frequencies is shown in Fig. 8.

The transit-time-factor T given by

$$T = \frac{\int_{gap} E(z) \cos\left(\frac{2\pi z}{\ell(n)}\right) dz}{\int_{gap} E(z)\, dz},$$

where E(z) is the electric field and $\ell(n)$ is the length of the n'th cell, can be obtained by carrying out numerical integration substituting the square roots of the frequency shifts for E(z). In Fig. 9, the results are plotted together with the MURA data. Though transit-time-factors were also obtained by using a smaller ball, they were not appreciably different from those in Fig. 9. Field distributions along the axis of the whole cavity were measured for the Type II cavity. Fig. 10 shows the analog output of frequency counter for zero-mode and for several higher modes.

We define the axial average field $\bar{E}(n)$ as

$$\bar{E}(n) = \frac{1}{\ell(n)} \int_{gap} E(z)\, dz. \qquad (2)$$

We plot the average field for the zero-mode in Fig. 11 and for higher modes in Fig. 12. The average field of the zero-mode was found to be constant along the axis. In addition, Fig. 12 shows that the average field has a simple cosine form,

$$\bar{E}(z_n) = \text{const} \cdot \cos\left(\frac{\pi \nu z_n}{L}\right), \qquad (3)$$

where L is the total length of the cavity, z_n is the position of the center of the n'th gap, and ν is an integer. Although the experimental results disagree slightly with the initial design given by equ. (1) for the zero-mode field, this gives a strong support to the normal mode analysis on the field excitations and distributions developed by one of the authors (T. N.)[5,7].

We also analyzed our results in terms of an equivalent circuit[6,7] as shown in Fig. 13. In this figure, C_n represents the gap capacity; $2 \times L_n/2$ the inductance which stores the magnetic energy surrounding the drift-tube and the gap; $C_{s,n}$ the capacitance between the drift tube and the outer cylinder; $2L_{s,n} \times 1/2$ the inductance between the adjacent stem-loops.

Neglecting $L_{s,n}$'s and $M_{s,n}$'s, we get relations between voltage V(n) and current I(n),

$$\frac{dV(n)}{dn} = -\left(j\omega L_n + \frac{1}{j\omega C_n}\right) I(n) \qquad (4\text{-}1)$$

$$\frac{dI(n)}{dn} = -j\omega C_{s,n} V(n). \qquad (4\text{-}2)$$

Then, we get an equation for I(n)

$$\frac{d^2I(n)}{dn^2} - \frac{1}{C_{s,n}} \frac{dC_{s,n}}{dn} \frac{dI(n)}{dn} +$$

$$\frac{C_{s,n}}{C_n} (\omega^2 C_n L_n - 1) I(n) = 0. \qquad (5)$$

When the resonant frequency of each cell is tuned to the zero-mode frequency as is the case of our model cavity, we obtain

$$L_n C_n = 1/\omega_0^2 . \qquad (6)$$

Now we consider the case of zero-mode. As the third term in equ. (6), we can easily solve the equ. (5). From the boundary consition at the end plate, $\left(\frac{dI(n)}{dn}\right)_{n=0} = 0$, we have I(n) = constant as long as $C_{s,n}$ has a finite value at n = 0. We can relate the axial average field $\bar{E}(n)$ to I(n) as follows,

$$\ell(n) \bar{E}(n) = \frac{I(n)}{j\omega_0 C_n} = -j\omega_0 L_n I(n). \qquad (7)$$

From the definition of L_n, we may assume that L_n is proportional to the cell-length as

$$L_n = k \ell(n), \qquad (8\text{-}1)$$

where k is a constant. Then, $\bar{E}(n)$ becomes constant and this is consistent with the results shown in Fig. 11.

Next we consider the higher modes. It is plausible that $C_{s,n}$ is also proportional to the cell-length. Therefore, we put

$$C_{s,n} = k' \ell(n), \qquad (8\text{-}2)$$

where k' is another constant. Using a relation $z_n = \int_0^n \ell(n)\, dn$ and equs. (6), (8-1) and (8-2), we rewrite equ. (5) in the form

$$\frac{d^2I(z_n)}{dz_n^2} + m^2 I(z_n) = 0, \qquad (9)$$

where

$$m^2 = k'k (\omega^2 - \omega_0^2). \qquad (10)$$

From the boundary condition, $\left(\frac{dI(z_n)}{dz_n}\right)_{z_n=0,L} = 0$ the solution of equ. (9) is given by

$$I(z) = A \cos(mz_n). \qquad (11)$$

Combining this with equs. (7) and (8-1), we get equ. (3) in agreement with the experiments.

We also measured field distributions on the axis for the stem-resonant mode. They are shown in Fig. 14. The frequency of the stem-resonance in each cell is given by[6]

$$\omega_{s,n} = \sqrt{\frac{1}{L_{s,n} C_{s,n}}} \sqrt{\frac{2L_{s,n}}{2L_{s,n} + M_{s,n}}} . \qquad (12)$$

Since $M_{s,n}$ will be proportional to the reciprocal of the distance between adjacent stems,

$$M_{s,n} = \epsilon \frac{L_{s,n} L_{s,n+1}}{\ell(n)}, \qquad (13)$$

where ϵ is a constant. Inserting equ. (13) into equ. (12), we have

$$\omega_{s,n} = \sqrt{\frac{2}{k' (2L_{s,n} \ell(n) + \epsilon L_{s,n} L_{s,n+1})}} . \qquad (14)$$

Since we used a uniform stem system, $L_{s,n}$ will be independent of the cell-length. Therefore, from equ. (14), we know that $\omega_{s,n}$ decreases as the cell-length increases. In the case shown in Fig. 14, the frequency is in passband for shorter cell-length, but is in stopband for longer cell-length. The phase shift per cell or per length is not defined in such a case. It is also noted that these results are consistent with the recent work by Dôme and White[7].

2. Model Study on Tank Fabrication

The accelerator tanks will be made by copper-plating the inner surface of mild steel cylinders. In this method, welding and large scale machining are limited only to the mild steel parts. After copper-plating, machining of the copper surface is not necessary. Thus, we are able to fabricate the tank at a lower cost. Three model unit cavities were made by this method. The dimensions of the unit cavity are as follows,

length of the unit cavity	500 mm	0.25 mm
diameter of the unit cavity	600 mm	0.1 mm
thickness of copper layer	1 mm	
surface roughness	< 10 μ	

The procedure of fabrication was as follows. After the end flanges and the other accessaries were welded on the mild steel cylinder and machining of the end flanges and the inner surface of the cylinder were performed, 1 mm thick copper layer was electro-plated on the inner surface of

the cylinder. During the copper deposition, the cylinder was rotated around its axis, and the copper surface was rubbed by ceramic edges. In this way, smooth and uniform copper layer was formed and farther finishing was not necessary. The measured Q-values of cavities consisting of n units are shown in Fig. 15, where the calculated values are also shown. As a result of vacuum tests no leaks were detected, (sensitivity of the He leak detector was 2.1×10^{-10} Torr/sec div) and an outgassing rate of 2.6×10^{-9} Torr/sec/cm^2 was measured.

A proto-type model of the first drift-tube as shown in Fig. 16 was made. This model has a shape of flat disc with rounded peripheries; 18 cm in diameter and 4.8 cm thick. The hole diameter is 2 cm. The tube consists of two half-cells, a Q-magnet holder with cooling passages, and a stem tubing. The cells are made of stainless steel and outer surfaces were plated with 1mm of copper. After the Q-magnet was mounted, the cells were sealed-off by means of an electron beam welder. The stem tubing was also made of stainless steel, copper plated and electron-beam-welded to the drift-tube body. It was found that such a process of fabricating drift tubes is most satisfactory.

References

1. MURA Linac Cavity Calculation: August 1964-July 1967.
2. D. Young, et al.: Proceedings of the 1966 Linear Accelerator Conference, Los Alamos, October 1966, p.115.
3. G. Parzen: Proceedings of the Sixth International Conference on High Energy Accelerators, 1967, A-34 .
4. S. Giordano and J. P. Hannwacker: Proceedings of the 1966 Linear Accelerator Conference, Los Alamos, October 1966, p.88 .
5. T. Nishikawa: Brookhaven Naional Laboratory Accelerator Department, Internal Report AADD-87, 1965 .
6. T. Nishikawa: Brookhaven National Laboratory Accelerator Department, Internal Report AADD-125, 1966 .
7. K. Batchelor, T. Nishikawa and T. Werntz: IEEE Transactions on nuclear science, Vol. NS-14, No. 3, June 1967, p.295 .
8. G. Dôme and I. White: Proceedings of the Sixth International Conference on High Energy Accelerators, 1967, A-19 .

Table I

Cavity diameter	:	94 cm
Drift tube diameter	:	18 cm
Hole diameter	:	2 cm
Radius of drift tube corner	:	2 cm
Radius of hole corner	:	1 cm

Table II

Cell Length Before Scaling Down (cm)	Dimension in this Experiment (Scaling Factor 88/94)		
	Cell Length (cm)	Gap Length (cm)	Drift Tube Diameter (cm)
6.22	5.83	1.24	
7.00	6.55	1.43	
8.00	7.48	1.69	
9.33	8.73	2.05	16.85
11.19	10.48	2.58	
13.99	13.10	3.44	
18.65	17.46	5.07	

DISCUSSION

(T. Nishikawa)

LAPOSTOLLE, CERN: I would first like to make a comment about the measurements of the frequency perturbation due to the stems. At CERN we tried to make such measurements on our models but we found for a low β structure that frequency perturbations, due to several stems, did not seem to add. The total effect depends upon the angle between the stems and various parameters. Also, I would like to ask a question, although this may not be appropriate to this session. Can anyone here explain why for an Alvarez structure, electrical breakdown always occurs in the low energy gaps while the peak field there is approximately the same, or even lower than in higher energy gaps?

(No answers)

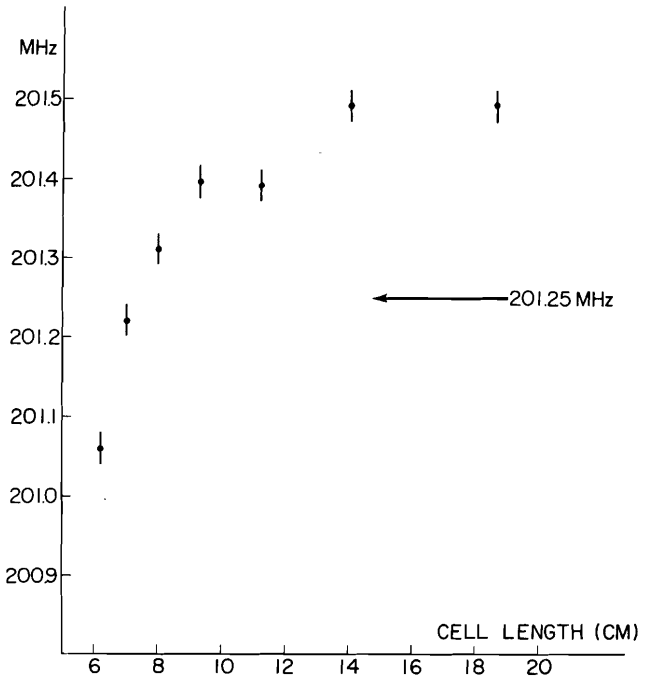

Fig. 1 Measured resonant frequencies of the unit-cells with stems. Vertical stem diameter 2 cm. Horizontal stem diameter 3 cm .

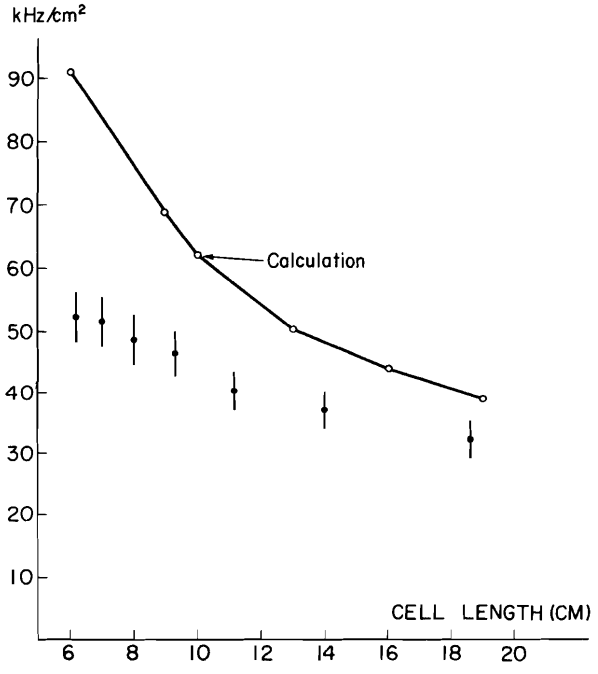

Fig. 2 Measured resonant frequency shifts per unit area of stem cross section. Curved line shows the calculated values[3].

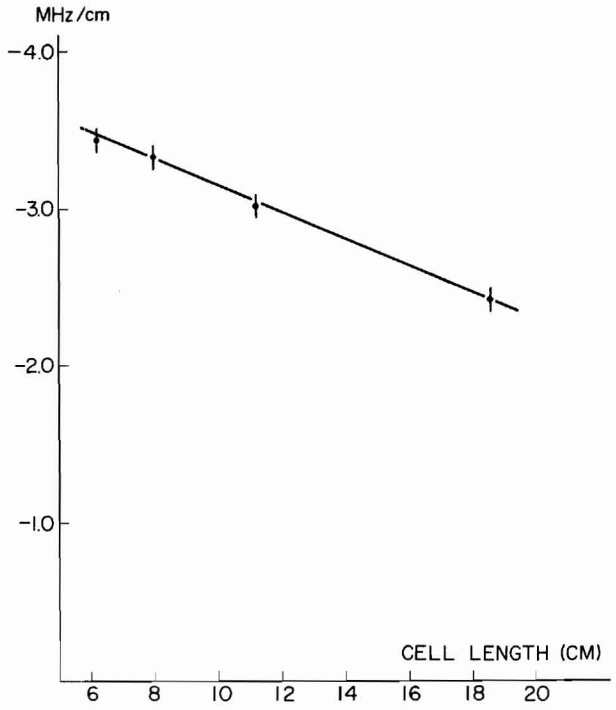

Fig. 3 Measured resonant frequency shifts due to small change of drift-tube diameter.

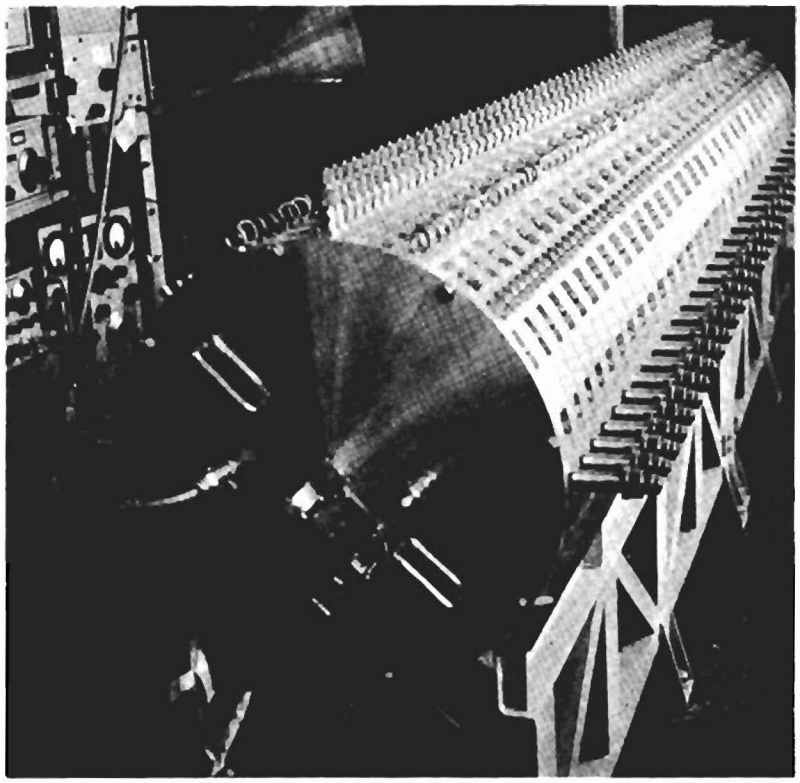

Fig. 4 Type II model cavity.

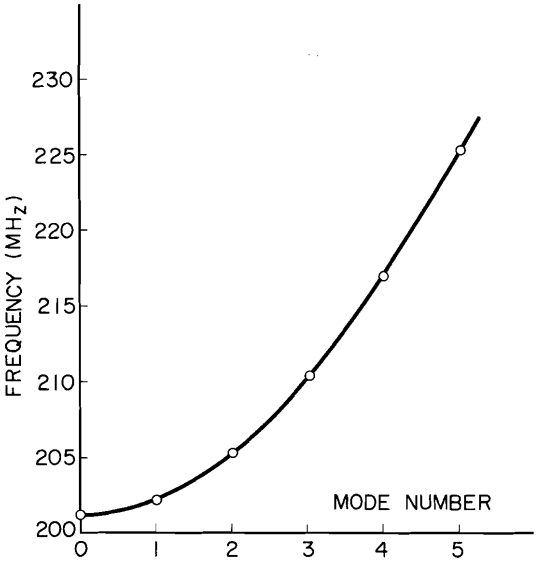

Fig. 5 Dispersion curve of the first tank.

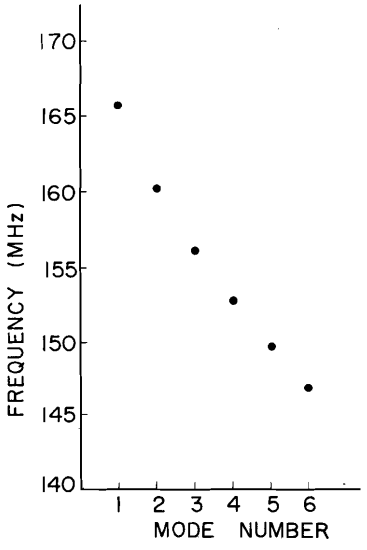

Fig. 6 Measured frequencies of stem resonances.

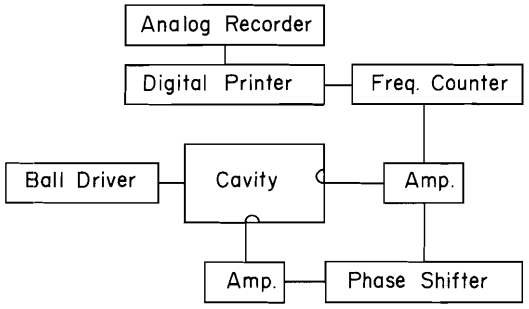

Fig. 7 Block diagram showing measuring system for axial field measurements.

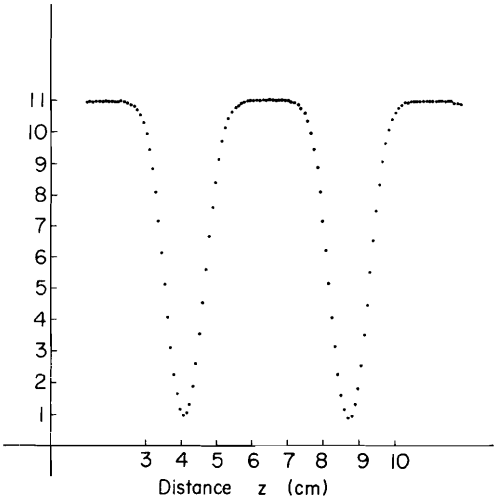

Fig. 8 Example of resonant frequencies perturbed by a 8 mm ϕ alminium ball on the axis of the Type I cavity.

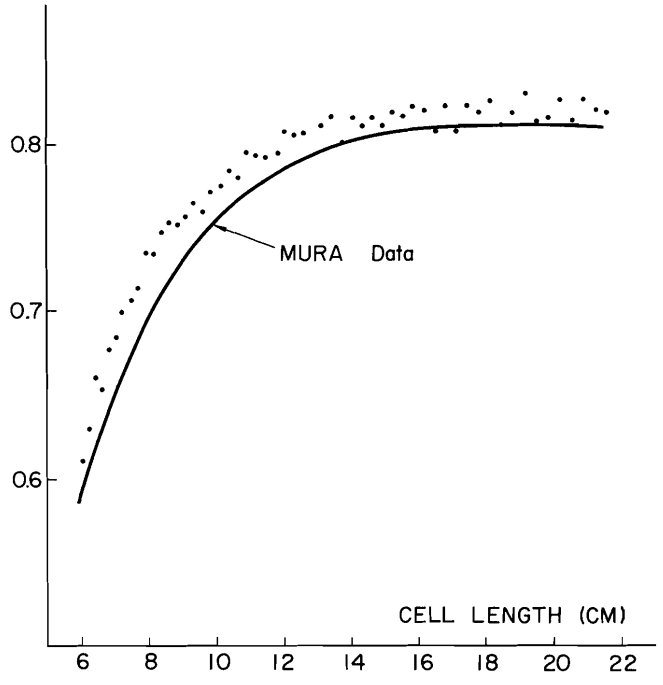

Fig. 9 Measured transit-time-factors. Curved lined shows transit-time-factors from MURA data.

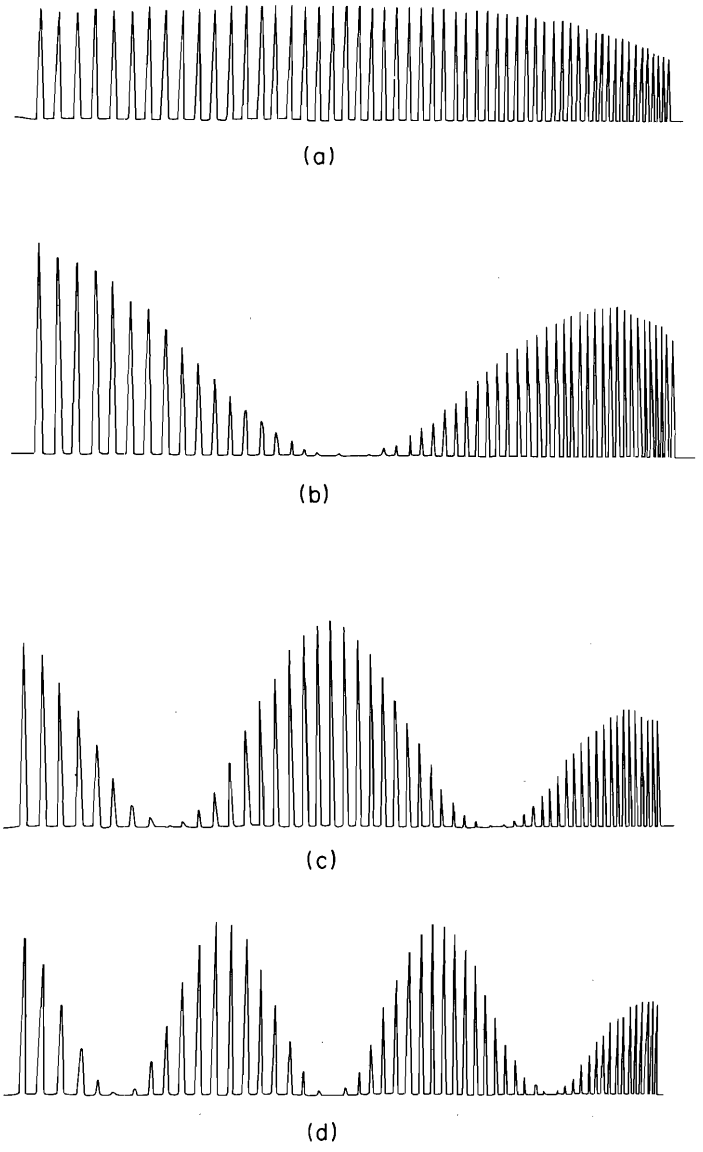

Fig. 10 Measured resonant frequencies perturbed by a alminium ball on the axis of the cavity. (a) TM_{010} mode (b) TM_{011} mode (c) TM_{012} mode (d) TM_{013} mode.

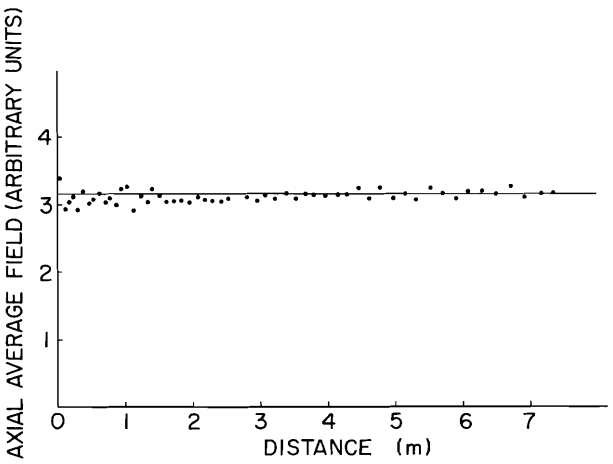

Fig. 11 Axial average field of zero-mode.

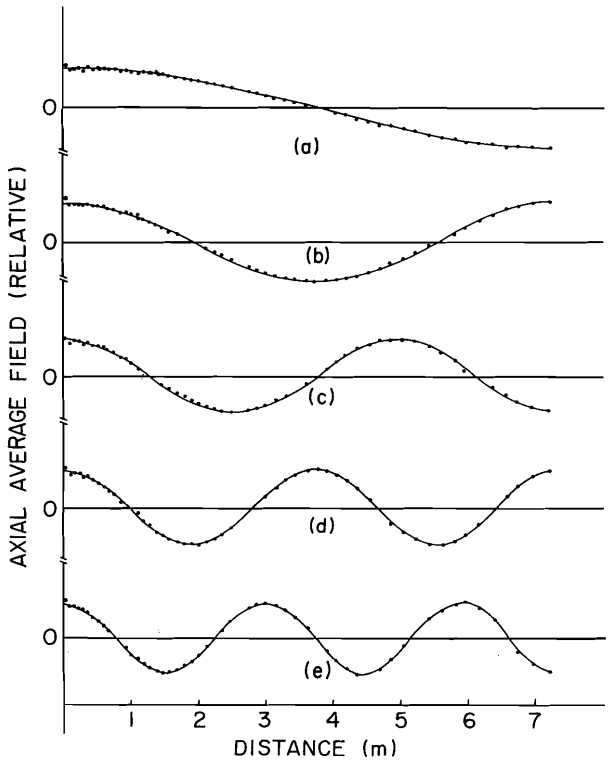

Fig. 12 Axial average field of higher modes.

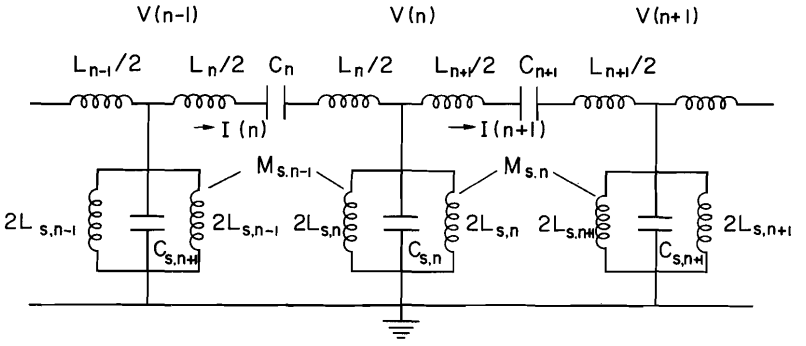

Fig. 13 Equivalent circuit for the linac cavity.

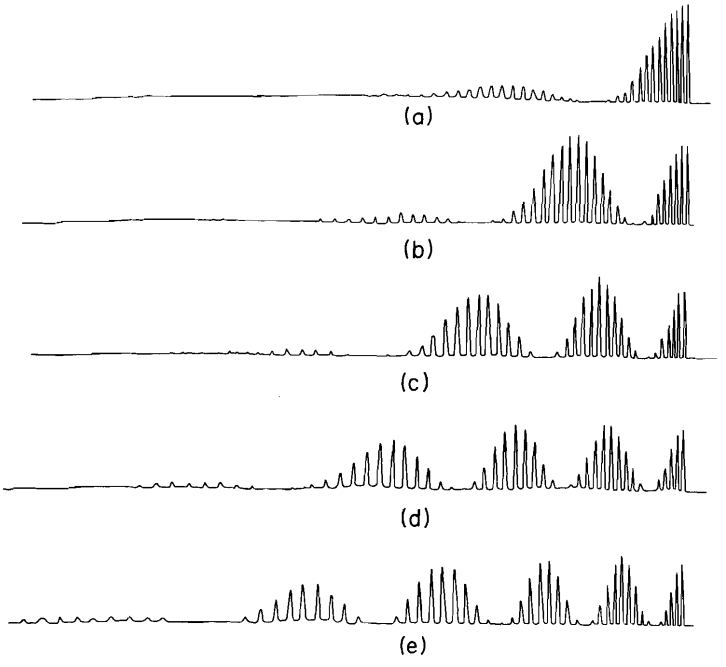

Fig. 14 Measured frequencies of stem-resonances perturbed by a alminium ball on the axis of the cavity.

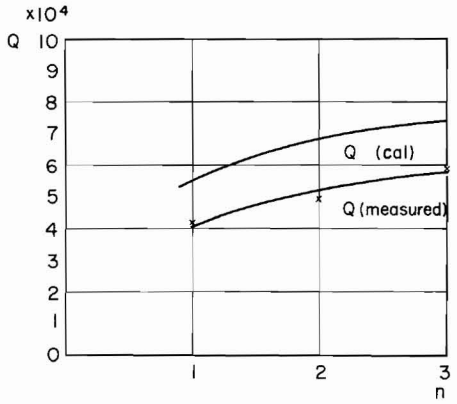

Fig. 15 Q-values of TM_{010} mode. Measured and calculated values for n units cavity.

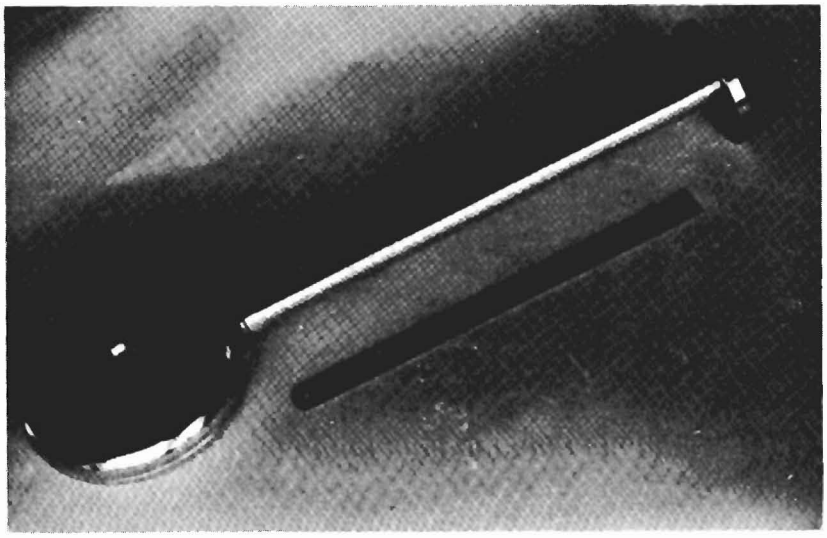

Fig. 16 A proto-type model of the first drift-tube.